CHAPTER 5

DEVICES INCORPORATING TRIS (8-HYDROXYQUINOLINATE) METALS

5.1 Preliminary

It was previously discussed in Chapter four that Mq3 materials are attractive to be applied in organic solar cells. This was revealed based on their characterization results, as they showed a unique optoelectronics, photophysical, structural and thermal properties. In this Chapter, the effect of incorporation of Mq3 into the devices active layers on the photo-absorption and overall performance of solution-processed ternary bulk heterojunction of DH6T/Mq3/PCBM are presented. At first and before the fabrication of devices, the absorption and photoluminescence behaviors of their active layers, with and without the addition of optimum Mq3, are investigated. Afterwards, devices with different architectural geometries are fabricated and assessed to identify the optimum structure of DH6T/PCBM thin films prior to the incorporation of optimum amount of Mq3 into the devices active layers.

Among the use of different organic materials in fabricating solar cells, intensive research work has been focused on the devices based on oligothiophenes and its derivatives (Millefiorini, et al., 2008; Ouhib, et al., 2008; Sakai, et al., 2009; Sun et al., 2006) as electron donors in one hand, and the fullerene materials (Jain et al., 2005; Oku, et al., 2008; Reyes-Reyes et al., 2007) as electron acceptors on the other hand. This is because of the high charge carrier mobility served by thiophenes (Chabinyc & Salleo, 2004; Cook et al., 2007; Koeppe & Sariciftci, 2006; Murphy, et al., 2004) and the deep electron affinity by fullerenes (Cook, et al., 2007; Koeppe & Sariciftci, 2006). Besides, through functionalizing thiophene chains (Bao & Lovinger, 1999) and buckminsterfullerene molecules (Wudl, 2002), their solubility can be improved. Upon addition of hexyl side chains to α-sexithiophene main molecule, dihexyl-sexithiophene

(DH6T) is obtained. DH6T is an organic semiconductor that has been mostly used in the organic field effect transistors (OFET) (Fraboni et al., 2009; Kwon & Seo, 2007; Nguyen et al., 2005; Ye, Baba, Suzuki, & Mori, 2008). The reported field-effect mobility of DH6T was found to be as high as 0.1 $cm^2.V^{-1}.s^{-1}$ (Murphy, et al., 2004), which is comparable to that of methanofullerene, PCBM (Cai, et al., 2010; Koeppe & Sariciftci, 2006). However, DH6T is the hole transport conductive, while PCBM is the electron transport one. Hence, the selection of DH6T/PCBM as host donor/acceptor active layers in the present studies is because of three major reasons; first, the nearly balanced charge transport mobility between DH6T and PCBM (for holes and electrons, respectively), second, the matched molecular energy level alignment between them (see Figure 2.15), and third, the lower cost of DH6T material compared to its polythiophene counterparts. All these can be helpful to realize cost effective solution processable organic solar cells, and to better understand the role of Mq3 incorporation due to the nearly balanced charge mobility between the donor (DH6T) and acceptor (PCBM) components. However, there has been no reported research work in the literature to investigate the photovoltaic performance of the organic solar cells based on DH6T/PCBM active layers. Besides, the exploitation of organic materials in fabricating solar cells is important for seeking the realistic and applicable photovoltaic effect, by the same mean, understanding the origin of their photovoltaic parameters (Djara & Bernède, 2005; Gupta, et al., 2010; Yamanari, et al., 2009) is highly desirable in achieving strategies for further improving these devices performance. The instruments used to characterize the blend films and to measure the photovoltaic performance of the devices for these studies are summarized below;

- Jasco V-570 UV-Vis-NIR spectrophotometer: Recording the photoabsorption response, hence estimating the absorption edges.

- LS50B Perkin Elmer luminescence spectrometer: Studying the photoluminescence behavior.
- Nicolet IS10-Thermo Scientific FTIR: Measuring the molecular absorptions.
- X-ray diffractometer (Bruker AXS): Studying the structural nature of the materials.
- KLA Tensor P-6 surface profilometer: Measuring the thickness of the films.
- Oriel solar simulator- model 67005: Supplying a standard light irradiation with intensity condition of 100 mW/cm^2, and AM 1.5 global reference spectra at room temperature.
- Keithley 236 source measurement instrument: Measuring the *I-V* characteristics of the devices in fourth quadrant region of the curve.

5.2 DH6T/Mq3/PCBM Heterostructure Films

In this Section, the effect of Mq3 incorporation on the absorption, photoluminescence, spectroscopic and structural properties of the photovoltaic active layers are discussed prior to the devices assessment and analysis.

5.2.1 Photoabsorption Response

The absorption spectra for pure DH6T and its doped states with different weight% of Mq3 (Alq3 or Gaq3 dopants) have been recorded in solution and film forms. It is seen that up to specific dopant content, this doping process has led to the shift in the absorption edge of the blends towards higher wavelengths (red-shift), thereby broadening the absorption spectrum of the mixtures. Figure 5.1 shows the absorption spectra of pure and doped DH6T solutions (5 mg/mL) prepared from carbon disulphide (CS_2) solvent. The addition of various weight percentages of Gaq3 into DH6T, clearly tuned the optical energy gap (E_g), which representing the fundamental absorption edge (E_{abs}), where photons are absorbed resulting in the electrons hopping from the ground

energy state (S_o) to the excited energy states (S_1). The blend mixtures of DH6T:Gaq3 are studied in these weight ratio sequences (1:0), (1:0.1), (1:0.3) and (1:0.5) that correspond to the weight percentages 0%, 9.1%, 23.1% and 33.3% of Gaq3. One can see from Figure 5.1 that from 0% to 23.1%, the absorption spectra are red-shifted, suggesting an increment in the π-bond conjugation lengths to excite more electrons into the excited states at lower photonic energies compared to that of the undoped states. Meanwhile, at 33.3%, the absorption edge is blue-shifted and a pronounced shrinking in the broad absorption band has been noticed. This may be due to the predominance of Gaq3 over DH6T molecules, thereby rendering the transfer of delocalized electrons between the DH6T and Gaq3 moieties, where lesser electrons in the hopping process from LUMO of DH6T to that of the Gaq3. The same results have been achieved once Gaq3 is added to DH6T, and no pronounce difference between the absorption spectra of DH6T/Alq3 and DH6T/Gaq3 systems can be observed, except that of their photoluminescence behavior, that will be discussed in the next sub-Section.

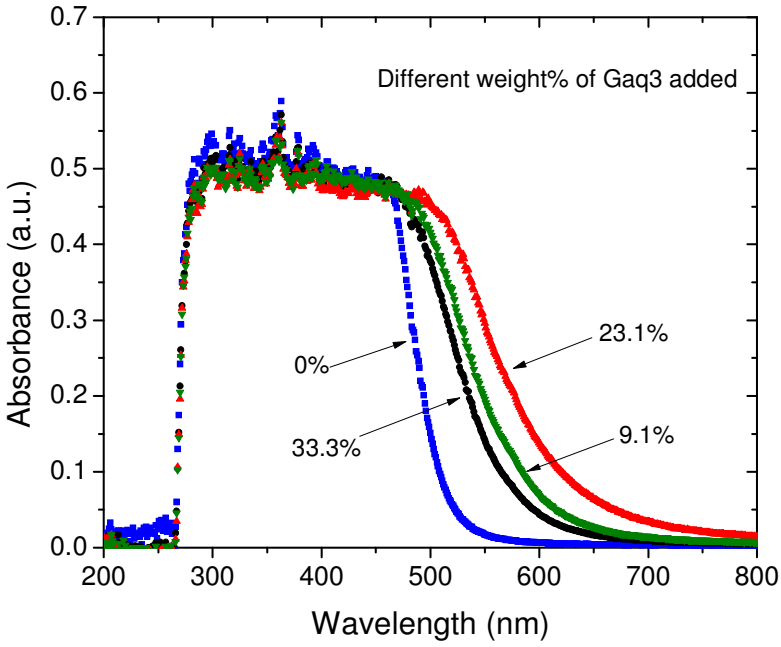

Figure 5.1: Absorption spectra of DH6T/Gaq3 blends: Influence of Gaq3 contents in DH6T solution.

Figure 5.2 shows a photograph of the material solutions prepared in vials. The solutions color was seen to change from nearly yellowish to the brown color upon adding Gaq3 into the DH6T solution. This evidence is qualitatively supporting the previous results, where the more brown solution indicates the more red-shift in its absorption spectrum.

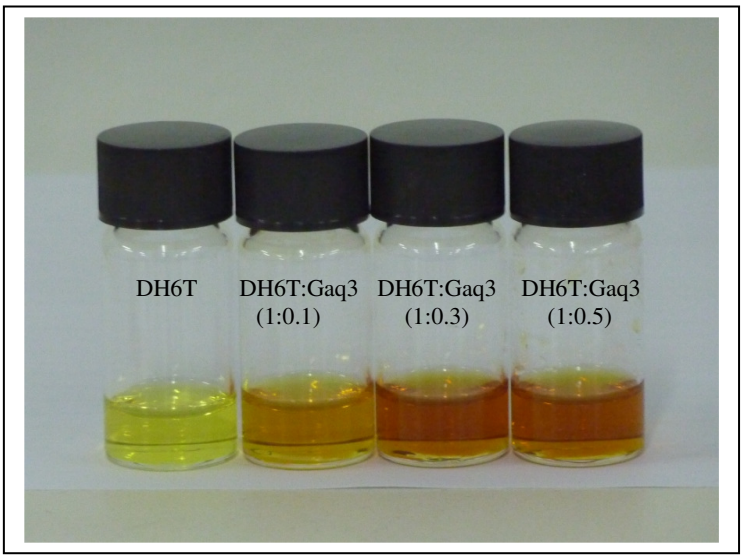

Figure 5.2: The DH6T:Gaq3 (1:X ratio) blend solutions prepared in the vials.

To estimate the effect of Mq3 addition on the absorption edge quantitatively, films of DH6T:Alq3, prepared from chloroform/hexane co-solvent, were deposited onto the quartz substrates to form thin films. By utilizing Equation 4.6, graphs of $(\alpha E)^2$ versus photon energy $E = h\nu$ for the DH6T:Alq3 films are plotted, as shown in Figure 5.3. Extrapolation of these plots to zero $(\alpha E)^2$ axis gives the fundamental absorption edge energy (E_{abs}). The influence of Alq3 content in the DH6T:Alq3 film possesses a similar trend to that in the solution form. However, for the solid state films, the absorption edge produces a considerable red-shift compared to that of the solutions. This can be attributed to the denser molecular packing in the film form that bears the stronger $\pi - \pi$ interchain interactions, favoring the lower optical band gap and weakly

bound delocalized electrons (Hernández, et al., 2009), while as in the solution form, intermolecular free rotation exists between the thiophene oligomers and molecular moities (Yassar et al., 1995), producing the higher optical band gap.

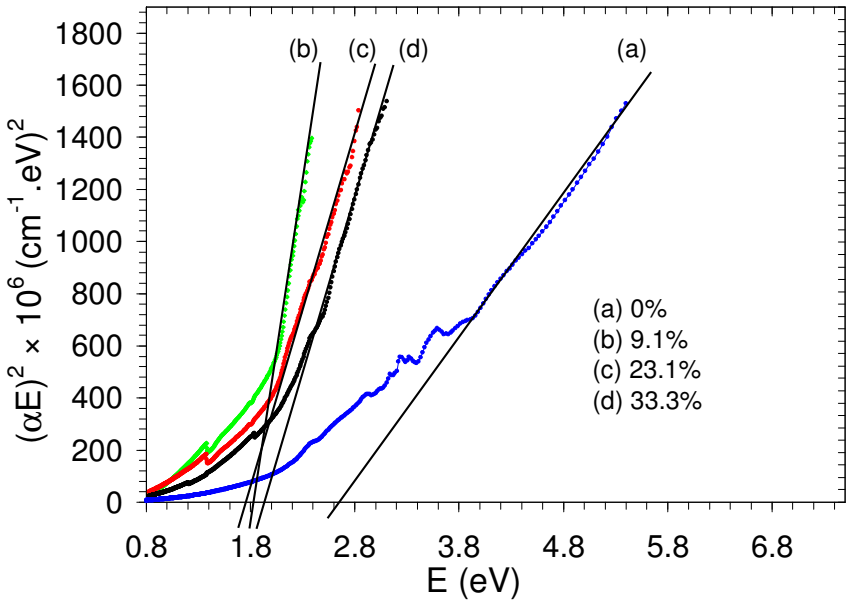

Figure 5.3: Plots of $(\alpha E)^2$ against photon energy E for the films of pure DH6T and DH6T:Alq3 blends.

The results illustrated in Figure 5.3 indicate a measurable effect of adding Alq3 on the absorption edge energy (E_{abs}) of DH6T:Alq3 with weight% of 9.1%, 23.1%, and 33.3% for Alq3, respectively. It is seen that E_{abs} decreases with increasing dopant content up to 23.1% then rises for higher concentration of 33.3%. The reduction in E_{abs} within the range of 0% to 23.1% is measured to be from 2.69 eV to 1.80 eV. This reduction in E_{abs} is attributed to the presence of intermolecular interactions between the DH6T chains (both backbone and side chains) and Alq3 ligands, where the aggregation of Alq3 molecules along the DH6T host becomes more prominent. The interactions may have two effects; an increase in the conjugation length which is brought about by the reduction in the absorption edge energy (shifting towards longer wavelengths), and a general effect on the dielectric constant (Bouarissa, 2007) of DH6T due to the added

presence of ions such as, O, N, and Al that is served by Alq3. But, the magnitude of the change is not linear in terms of its dependence on dopant concentration. It is clear that for the concentration ranging from 0% to 9.1% has caused the E_{abs} to decrease from 2.69 to 1.88 eV, producing an energy difference of 0.89 eV. While as, a further variation in concentration from 9.1% to 23.1% has led to a small modification in the E_{abs} (1.88 eV to 1.80 eV). This nonlinearity may be due to trends toward a saturated interaction (in terms of the available geometrical positions) between the chains of DH6T host and aggregated molecular ligands of Alq3. Upon adding higher concentrations of Alq3 (above 23.1%), the value of the absorption edge energy started to rise to the larger value of E_{abs} = 1.94 eVt. This may be because of the appearance of predominated Alq3 over the DH6T components, as Alq3 corresponds to the higher E_{abs} (of about 2.86 eV) compared to that of the DH6T host (2.69 eV).

To determine the optimum amount of Mq3 to be mixed with DH6T in order to give the highest red-shift in the absorption spectra of their films, an attempt has been performed to find a formula, which fits the experimental findings. Figure 5.4 shows a plot of E_{abs} versus molar concentration of Alq3. The symbols represent the experimental data, while the continuous line represents the empirical formula. The curve shown in Figure 5.4 is best fitted the experimental data with the following formula:

$$E_g = E_{g1}\left(\frac{1-x}{1+Bx}\right)^2 + E_{g2}\left(\frac{(1+2B)x}{1+2Bx}\right)^2 \tag{5.1}$$

where, B is a numerical factor, B=1.6, E_{g1}, E_{g2}, and x denote the absorption edge energies of DH6T host (2.69 eV), added Alq3 (2.86 eV), and the molar fraction of Alq3, respectively. Based on the fitted curve, the optimum amount of Mq3 to yield the lowest E_{abs}, which is important in the organic solar cells consideration, is predicted to be about 25%.

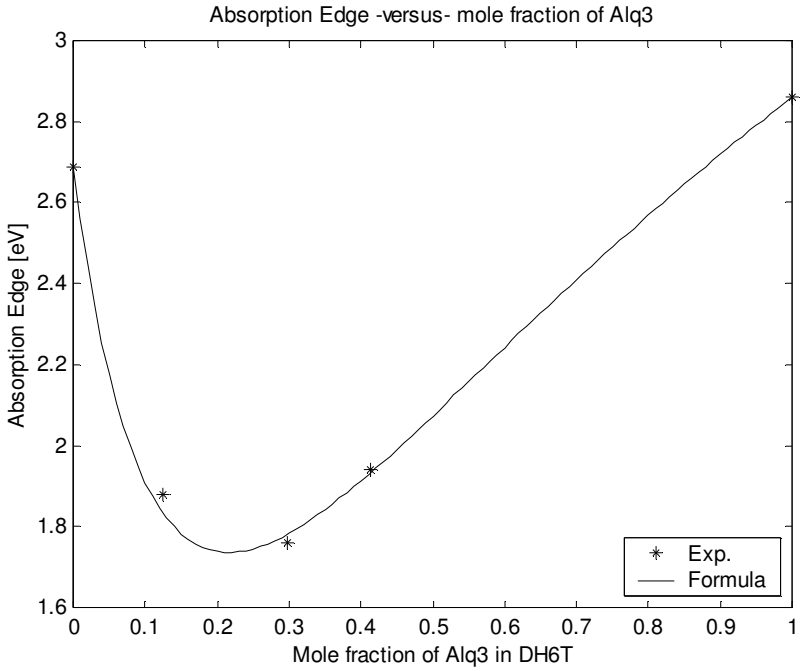

Figure 5.4: Plot of DH6T:Alq3 absorption edge energy versus molar concentration of Alq3.

After speculating the optimum amount of Mq3 dopant to be added into the Pristine DH6T to obtain the broadest absorption spectra, photovoltaic active layers based on DH6T/Mq3/PCBM ternary bulk heterojunction films, prepared from carbon disulphide (CS_2) solution, were spin coating onto the glass substrates for the optical characterization purpose. Figure 5.5 shows the normalized absorbance of the coated films together with DH6T, PCBM, and their blend films. The pristine DH6T reveals an absorption band of about 370 nm and the PCBM acceptor around 340 nm, which are close to those reported by Cook, et al. (2007); and Kwon & Seo (2007). Nevertheless, these bands overlap with only a small portion of the solar spectrum with a photon flux peak around 700 nm. Upon bringing the materials into contact to form the bilayer (BL) or bulk heterojunction (BHJ) films, however, less red-shift in the absorption edge characteristics compared to that of the host DH6T has been achieved, but the bulk heterojunction films show larger red-shift than that of bilayer films. This could be one of the reasons of better photovoltaic performance in the bulk heterojunction devices

compared to that of the bilayer cells, as it will be discussed later. The red-shift in the absorption spectra of DH6T:PCBM blends with respect to that of DH6T indicates the enhanced photo-induced charge transfer that is brought about by the closer proximity between the donor-acceptor molecules (Koeppe & Sariciftci, 2006). The curve shape consistency for the films with the absorption spectra of PCBM from 250 nm to around 350 nm may be resulted from the stronger intermolecular interaction between DH6T and PCBM molecules in this range, as PCBM triplet photoexcited state absorbs light more efficiently than its ground state (Wudl, 2002) and the first excited state is mostly symmetry forbidden with only transitions at higher energies are fully allowed (Cook, et al., 2007; Koeppe & Sariciftci, 2006). Similarly, the weak tails to their absorption spectra extending as far as 700 nm (1.77 eV) is thought to be originated from the PCBM. Of great interest is the photoabsorption enhancement due to the incorporation of Mq3 materials into the active layers. The inclusion of Gaq3 or Alq3 has made the absorption spectra to red-shift towards 700 nm or above, revealing that the most significant contribution of Mq3 to the spectral response occurs when both of DH6T and PCBM are present in the form of ternary DH6T/Mq3/PCBM bulk heterojunction. This broadened spectrum is attributed to the contribution of the ternary components in adjusting the molecular energy levels to yield an efficient charge transfer and theoretically higher photocurrent generation, thereby harvesting larger amount of photons. Noteworthy, upon incorporating Gaq3, relatively broader spectrum has been obtained, could be due to the matching of energy level alignment between DH6T/Gaq3/PCBM components (see Figure 2.15). This larger harvesting of light due to the incorporation of Mq3 is considered to be one major reason for efficient device fabrication, as it will be seen later that devices with introduced Mq3 produce interest improved photovoltaic performance over those without Mq3.

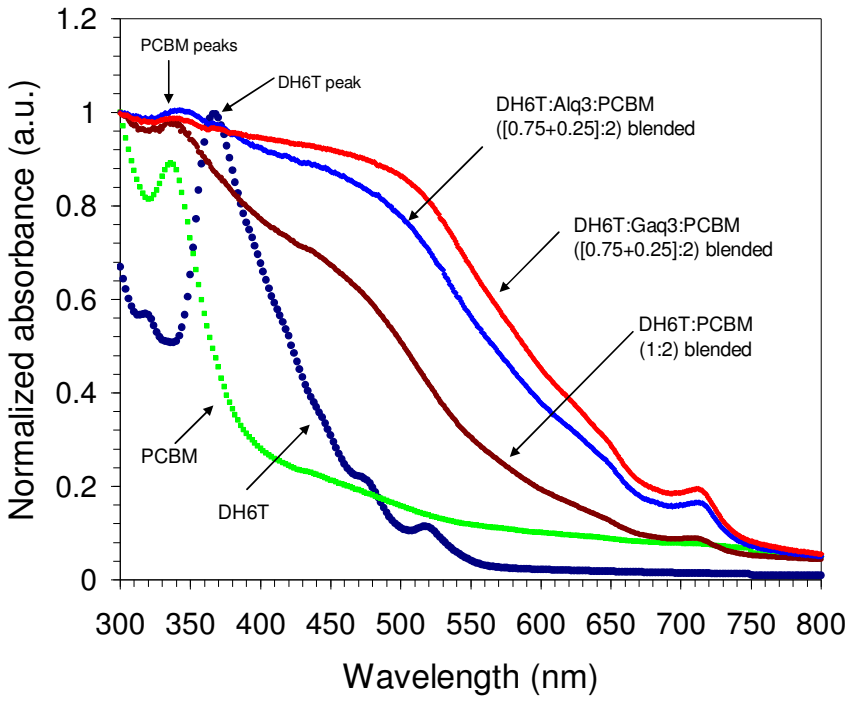

Figure 5.5: Normalized absorbance of DH6T, PCBM and DH6T/PCBM blend films with and without incorporating Mq3.

5.2.2 Photoluminescence Behavior

Figure 5.6 shows the PL spectra of pristine DH6T and DH6T/Mq3/PCBM donor-acceptor blend films excited at wavelength source of 360 nm. Luminescence property of materials is a direct measure to the probability of radiative charge recombination. As a matter of fact radiative recombination occurs after exciton migration towards low energy traps (probably at the grain boundaries) whose emission efficiency is high due to the weak intermolecular interactions (Sassella et al., 1999). The PL spectra of pristine DH6T shows two characteristic peaks, one relatively sharp at about 400 nm and another broad peak in the visible region centered at approximately 550 nm. This is close to that observed for DH6T in chloroform solution (Kwon, Chung, Oh, Bae, & Ju, 2009; Kwon & Seo, 2007). Such a dual PL property of thiophene based organics is a common feature (Sato, Fujitsuka, Segawa, et al., 1998), as it depends on the conjugation length of the thiophene oligomer and on the substituent introduced to the chain. As presented in

Figure 5.6, the PL spectrum of DH6T demonstrates a shape with equally spaced peaks separated by about 15 nm (0.9 eV). Such a feature is usually interpreted as a vibronic coupling of the electronic transitions (Horowitz, et al., 1997; Loi et al., 2001). Upon the addition of Mq3 and PCBM acceptors into the DH6T, the PL intensity faced a reasonable decrease in radiative recombination of the generated excitons due to excitation. Beside, the broad PL within visible region slightly shifted to a lower energy (higher wavelength) compared to that pristine DH6T, implying that the effective conjugated length of the segment responsible for PL is longer in the DH6T/Mq3/PCBM ternary blended films. However, the exciton formed in the segment of shorter conjugation length, e.g. sexithiophene, should immediately migrate to the segment with longer conjugation length (Sato, Fujitsuka, Segawa, et al., 1998). Thus, almost the same PL spectra are observed for both pristine DH6T and DH6T/Mq3/PCBM blend despite the difference in their absorption spectra. The quenched PL activity is therefore a strong indication of facilitating efficient charge transfer from the pristine DH6T to the Mq3/PCBM acceptor, making this ternary blended film is attractive to be exploited in organic solar cells. A significant PL quenching has been observed when Gaq3 is introduced to the films instead of Alq3. This can be safely ascribed to the most matched energy HOMO and LUMO energy levels alignment between DH6T/Gaq3/PCBM components compared to that of DH6T/Alq3/PCBM, allows easier pathway in transporting of excitons, thereby reducing the radiative decaying probability, i.e., lower photoemission spectrum. One more reason might be the higher refractive index of Gaq3 compared to that of Alq3, as more excitons can be dissociated at the donor-acceptor boundaries as a consequence of generated stronger internal electric field and space charge accumulation upon illumination (Chan, Ng, 1998). Nevertheless, no emission of Mq3 for 25% doping concentration was observed, suggesting that the energy transfer

from Mq3 to DH6T is nearly absolute due to relatively low Mq3 dopant concentration in the blends.

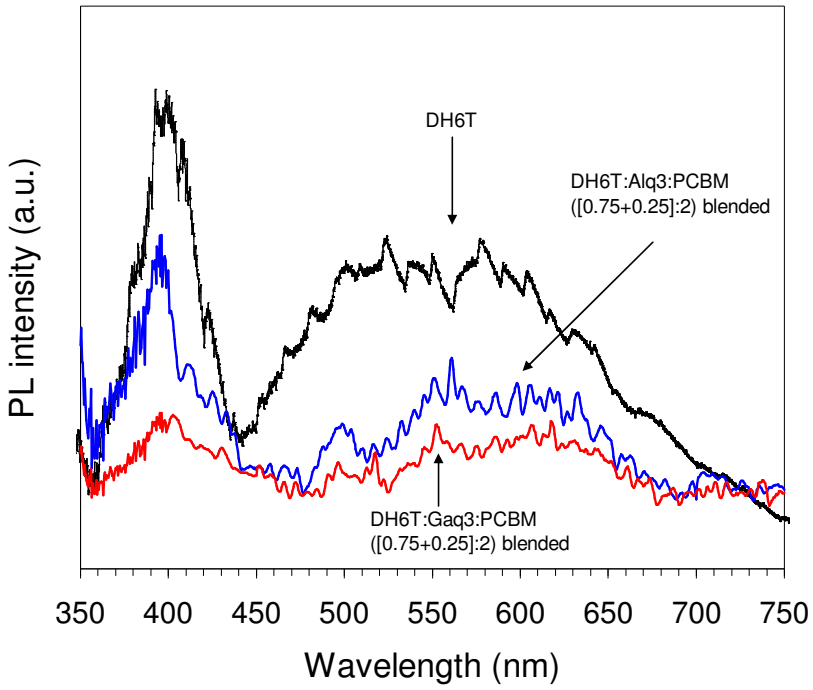

Figure 5.6: Photoluminescence spectra of DH6T, DH6T/Alq3/PCBM and DH6T/Gaq3/PCBM films excited at 360 nm.

5.3 Devices Based on DH6T/PCBM Bilayer and Bulk Heterostructure

In this Section different photovoltaic device geometries are discussed and analysed in order to understand and to estimate the most efficient design to be selected for the purpose of incorporating the Maq3 materials in the devices. According to the devices architecture, the solar cells are divided into three types and labeled as A, B and C, which corresponds to DH6T/PCBM (BL), PEDOT:PSS/DH6T/PCBM (BL) and PEDOT:PSS/DH6T:PCBM (1:1 BHJ) respectively. In this case, BL refers to the bilayer and BHJ refers to the bulk heterojunction structure. From each of the labelled groups, seven devices have been tested and assessed. So, the presented graphs throughout this

paper are sketched from the average of the measured data. Figure 5.7 shows the *J-V* characteristics of those solar cells, while Table 5.1 tabulates the achieved photovoltaic parameters. Among the bilayer structures, device B shows better performance to that of A, such that the short-circuit current density (J_{sc}) has been increased from 0.027 to 0.040 mA.cm^{-2} and the open-circuit voltage (V_{oc}) enhanced from 0.18 to 0.24 V. By these means, the power conversion efficiency (η) and fill factor (*FF*) have also been increased. The overall conversion efficiency of the devices with the presence of PEDOT:PSS layer between ITO and active layers in device B is seen to be improved by 100% compared to that of non-introduced PEDOT:PSS layer in device A.

Table 5.1: The average value of the obtained photovoltaic parameters for the studied organic solar cell devices.

Device	$J_{sc.}$ **(mA)**	$V_{oc.}$ **(V)**	$P_{max.}$ **(µW)**	V_{mp} **(V)**	V_{oc}/V_{mp}	***FF* %**	**η %**
A	0.027	0.18	1.6	0.11	1.63	33	0.002
B	0.040	0.24	3.5	0.15	1.60	36	0.004
C	0.097	0.36	8.5	0.19	1.90	24	0.01

Such improvement in the photovoltaic performance is due to reduction in the junction resistance across the ITO/DH6T interface in the presence of the PEDOT:PSS interlayer, which results in an improved hole carrier transport. The improvement of the photovoltaic performance of organic solar cells by introducing the PEDOT:PSS layer was also claimed by other researchers (Bernède, Derouiche, & Djara, 2005; Yeon Song, Kim, & Kim, 2005). Despite that the thickness and interface characteristics determine the efficiency of the devices (Nodari, Koehler, da Luz, & Roman, 2005), the overall conversion efficiency is not optimized in absolute terms with respect to the films thickness in this study. This is to guaranty a comparative study between the devices, i.e. determining the difference in the photovoltaic performance between the double layer and blended type of devices. Hence, the comparison between devices B and C is

consequently being targeted. In this case, device C exhibited a significantly improved photovoltaic effect performance (see Figure 5.7 and Table 5.1). The J_{sc} has increased from 0.040 to 0.097 mA.cm^{-2} and V_{oc} from 0.24 to 0.36 V, respectively. So, the power conversion efficiency enhanced by 150% of that obtained in device B. This analysis is safely ascribable to the photon absorption extended to the longer wavelength by the BHJ film and better proximity between the donor and acceptor molecules. It should be recalled that the charge separation takes place only at donor/acceptor (D/A) interface. Since the exciton (bounded electron-hole pair) diffusion length is only in the order of 10 nm, the charge generation can only occur if the dissociation site is located within this distance. This means, in the case of bilayers, only a small domain near the D/A interface is active, therefore the generated current is small. On the other hand, in the case of bulk heterojunction, the charge separation can take place within the whole bulk of the organic layer (Chu, et al., 2011; Yasuhiko Hayashi, et al., 2008; Reyes-Reyes, López-Sandoval, Liu, et al., 2007). Hence, larger current can be generated.

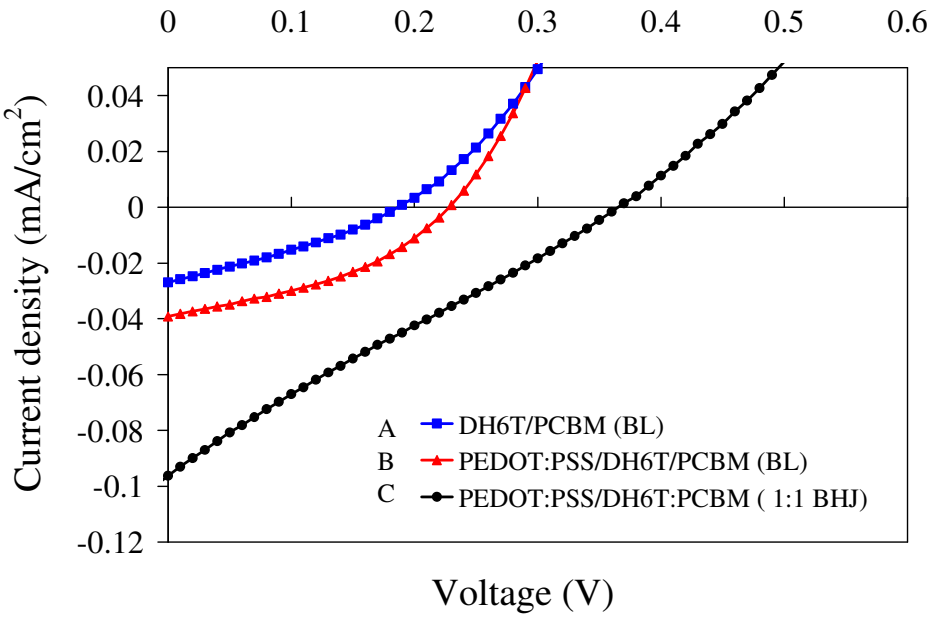

Figure 5.7: The *J–V* characteristics of the organic solar cells with device A- DH6T/PCBM (BL), device B- PEDOT:PSS/DH6T/PCBM (BL) and device C- PEDOT:PSS/DH6T:PCBM (1:1 BHJ)

Another noteworthy result is one which observed in the fill factor, *FF* of the BHJ cells, device C; that despite of better photovoltaic performance and power conversion efficiency, the value of *FF* is smaller (0.24) compared to that of devices A and B (with *FF* of 0.33 and 0.36, respectively). For more elucidation, graphs of Power density-Voltage (*P-V*) characteristics are plotted, as shown in Figure 5.8, and the measured V_{oc}/V_{mp} ratio is tabulated in Table 5.1. V_{mp} is the operating voltage of the solar cell devices at a maximum power point (MPP) that is capable to be delivered from the cells. *FF* is calculated by dividing this power value over the product of open circuit voltage and short circuit current (V_{oc} x J_{sc}). One can notice that the value of V_{mp} is enlarged with increasing the V_{oc} in the following sequence of the investigated devices: A < B < C. If a standard *P-V* characteristic curve is considered, then the ratio of V_{oc} to V_{mp} should be relatively constant. But, in the current study this ratio (V_{oc}/V_{mp}) is found to be 1.63, 1.60, and 1.90 for devices A, B, and C, respectively (see Table 5.1). Therefore, the A and B devices follow this rule, while device C is deviated from this standardization. This evidence can also be seen from the geometrical shape of the *P-V* curves, where for the BHJ structure (device C), the shape of the curve is semicircle (centered at V_{mp}) but semi-ellipse for the others. One of the reasons for this deviation by the BHJ devices is more likely to be originated from the architectural geometry of the devices. It is thought that the nanoscale morphology in the bulk donor/acceptor active layer is more complicated to be controlled well in terms of the phase separation between the donor and acceptor regions (Djara & Bernède, 2005). Hence, very likely leakage current persistence due to the insufficient contact of the acceptor phase with the cathode and donor phase with the anode electrodes.

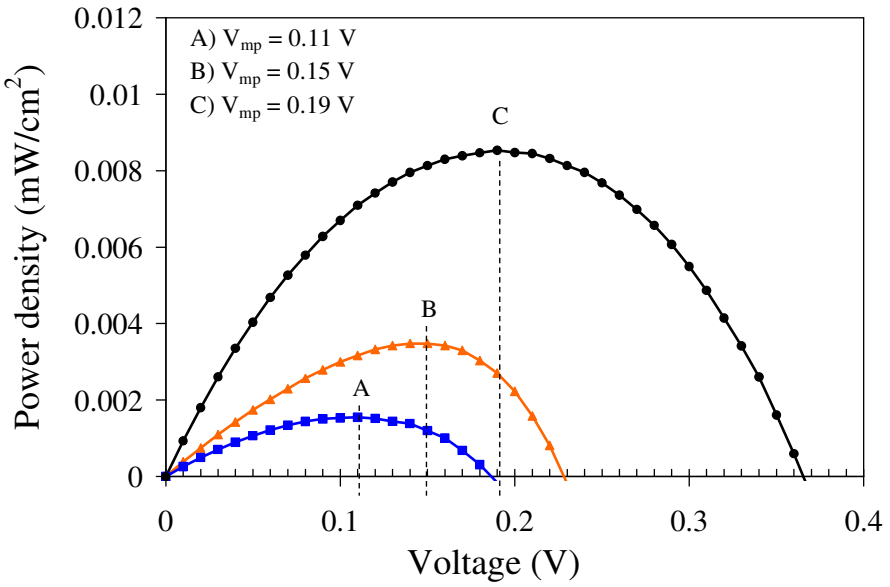

Figure 5.8: The *P–V* characteristics of the organic solar cells composed of A-DH6T/PCBM (BL), B- PEDOT:PSS/DH6T/PCBM (BL) and C-PEDOT:PSS/DH6T:PCBM (1:1 BHJ) active layers.

One more parameter affecting *FF* is the series resistance, R_s of the cell that can be correlated by (Tej Mallajosyula, Srivastava, Sundar Kumar Iyer, & Mazhari, 2010):

$$FF = FF_o(1 - R_s \frac{J_{sc}}{V_{oc}}) \tag{5.2}$$

The higher *FF* of device B compared to that of device A can be referred to the decrease in R_s through the insertion of PEDOT:PSS layer, as the value of J_{sc}/V_{oc} for the A and B devices in Equation 5.2 is 0.15 and 0.16 $m\Omega^{-1}$ respectively. Noticeably, the later value is a bit higher, means that the R_s must have been decreased to raise the *FF*. Moreover, the decrease in *FF* for device C is not necessarily due to its high R_s compared to that of A and B devices. Otherwise, it is entirely due to the deviation from the standard *P-V* characteristics shape as discussed above and is governed substantially by the morphological issues in the BHJ device. The high J_{sc}/V_{oc} value of approximately (0.23 $m\Omega^{-1}$) that is quite enough to lower *FF* down to 0.24 can also support the previous clarification.

Two major approximations have been mentioned to understand the origin of V_{oc} in the organic solar cells (Yamanari, et al., 2009), the first perspective based on the metal-insulator-metal (MIM) theory giving V_{oc} as the difference in the work function of the cathode and anode electrodes, while the second viewpoint derived from the difference in the Highest Occuppied Molecular Orbital (HOMO) of the donor and Lowest Unoccuppied Molecular Orbital (LUMO) of the acceptor for estimating V_{oc}. Based on MIM and HUMO-LUMO theories, the limit of V_{oc} of the devices can be approximately 0.6 V and 1.3 V, respectively (see Fig.3.24-d on page). As the achieved V_{oc} was 0.36 V for the BHJ devices; suggesting that still further improvements possible to be performed to get a higher V_{oc} and better photovoltaic performance.

5.4 Devices Based on DH6T/Mq3/PCBM Ternary Bulk Heterojunction

In this Section, the photovoltaic and electrical measurements performed upon devices with and without incorporated Mq3 materials, as a ternary bulk heterojunction of DH6T/Mq3/PCBM, are presented and discussed. Figure 5.9 below shows the architectural structure of these devices.

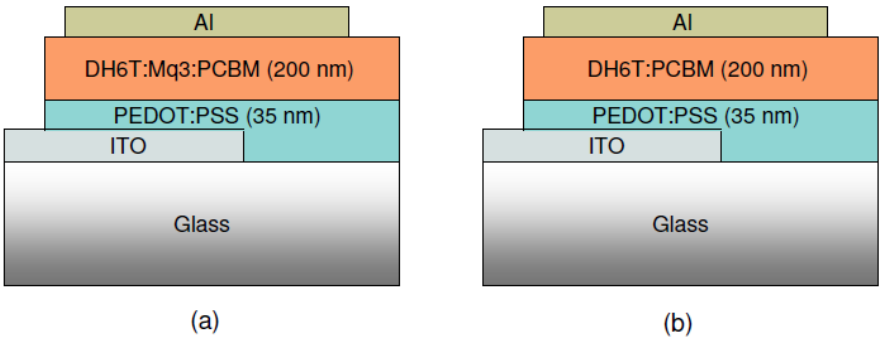

Figure 5.9: Device structures of (a) DH6T:Mq3:PCBM ternary bulk heterojunction, and (b) DH6T:PCBM bulk heterojunction devices.

5.4.1 Current-Voltage and Power-Voltage Characteristics

Figure 5.10 shows the current density versus voltage characteristics of the devices fabricated with and without incorporating Gaq3 or Alq3 into the devices active layers. The results show a significantly enhanced photocurrent and overall photovoltaic performance upon the addition of Mq3 compared to those of non-included Mq3 devices, i.e., DH6T/PCBM (1:2) based devices. Such that, upon the addition of Alq3, the short current density is increased from 0.63 mA to 1.06 mA and the open circuit voltage increased from 0.30 V to 0.60 V; alternatively, by incorporating Gaq3 these enhancements are seen to be higher in comparison to those of Alq3-based. The addition of Gaq3 facilitated an increment in I_{sc} from 0.63 mA to 1.26 mA, while V_{oc} considerably increased from 0.30 V to 0.75 V, in reference to those of without Gaq3 devices. By this, the I_{sc} and V_{oc} have been increased by factors of 2 and 2.5, respectively. These improvement in I_{sc} is attributed to the enhancement in the light harvesting due to the complete photo-absorption in the wavelength range from 250 nm to 450 nm by Mq3 specifically, where DH6T and PCBM absorb the light weakly, and the broadened absorption spectrum of the whole active layer to about 700 nm due to the Mq3 incorporation, more generally (see Figure 5.5).

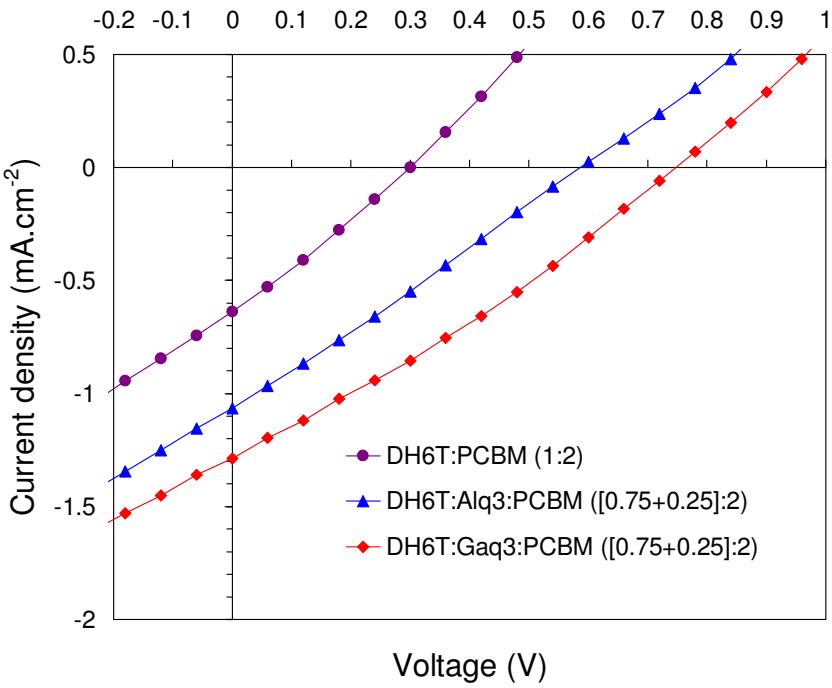

Figure 5.10: The *J–V* characteristics of the bulk heterojunction devices with and without incorporated Mq3.

It is worth mentioning that by incorporating Gaq3 a better photovoltaic performance has been achieved. This can be referred to the most promising photophysical properties of Gaq3 compared to those of Alq3, as explained thoroughly in Chapter four. Besides, the HOMO and LUMO levels in the DH6T/Gaq3/PCBM system are more preferably aligned than that of the DH6T/Gaq3/PCBM system. As shown in Figure 5.11-(a), the descending arrangement pattern in the LUMO and HOMO levels of DH6T/Gaq3/PCBM system in the sequences of (3.9 > 3.0 > 2.9) eV, and (6.0 > 5.8 > 5.2) eV, respectively, facilitates efficient electron transfer from the LUMO of DH6T to that of PCBM through that of Gaq3, and reasonable hole transfer from the HOMO of PCBM to that of DH6T via that of Gaq3. This is ultimately acts upon increasing the photogenerated charge carriers that are collected by the respective electrodes (ITO and Al), thereby I_{sc} has been enhanced. Additionally, this proper energy bands alignment will reduce the probability of electron-hole recombination, which in turn producing effective PL quenching for the blends containing Gaq3 compared to that of Alq3-based

(see Figure 5.6). A reduction can be noticed in the energy levels alignment in the HOMO of DH6T/Alq3/PCBM system, as shown in Figure 5.11-(b), from the high HOMO value of Alq3 (6.30 eV), which is below to that of PCBM (6.0 eV) by a difference of 0.30 eV. This inappropriate energy levels alignment assists some of the generated holes to take their path towards PCBM rather than DH6T, which consequently leads to higher electron-hole recombination and PL increment, compared to that of DH6T/Gaq3/PCBM films. Moreover, based on the $(HOMO)_D$-$(LUMO)_A$ estimation for V_{oc}, the 0.3 eV difference at the boundaries of Alq3/PCBM may play the role of weakening the electric field responsible to dissociate excitons and charge carriers collection, thereby lowering the V_{oc} of the devices. As such, the devices based on DH6T/Alq3/PCBM show smaller V_{oc} (0.60 eV) compared to that of DH6T/Gaq3/PCBM (V_{oc} = 0.76 eV). However, the origin of V_{oc} has been remained matters of debate and controversial so far. Of great importance is the reproducibility feature; interestingly, devices with incorporated Mq3 revealed almost the same characteristic behavior for a set of similar devices even when they have been tested over several times of photovoltaic measurements. Hence, the average results are obtained from the measurements performed on four devices.

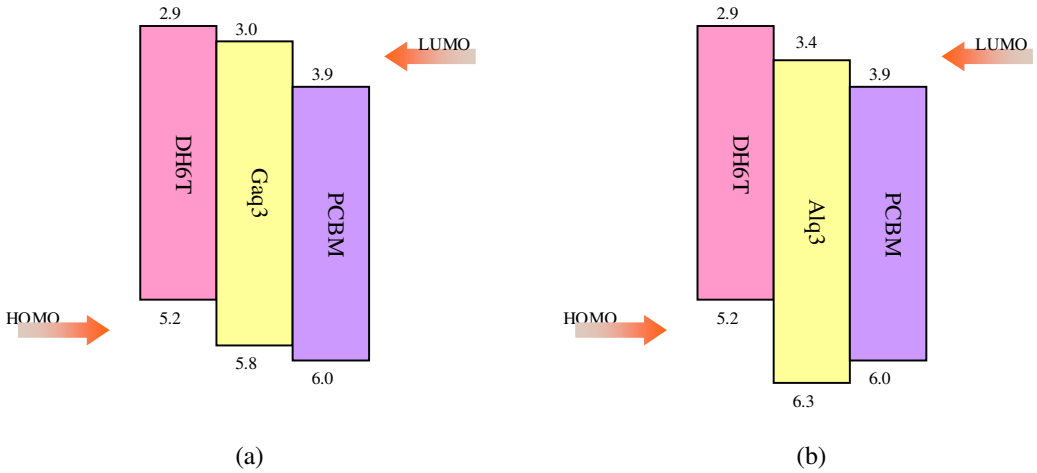

Figure 5.11: The HOMO and LUMO energy levels alignment between the DH6T/Gaq3/PCBM (a) and DH6T/Alq3/PCBM (b) ternary bulk heterojunction active layers.

Figure 5.12 shows the power density versus voltage characteristics of the devices fabricated with and without incorporating Gaq3 or Alq3. The results show an enhanced output power from 0.05 mW to 0.17 mW for the Alq3 incorporated devices, and from 0.05 mW to 0.28 mW for the Gaq3-incorporated. The devices were illuminated under about 100 $mW.cm^{-2}$ light intensity. The power conversion efficiency was seen to increase from 0.06% to 0.21% and from 0.06% to 0.35% for the Alq3 and Gaq3 based devices, respectively. As such, the output power and efficiency of the devices has been improved by a factor of approximately six times greater than that of devices fabricated without the addition of Mq3. Nevertheless, the *P-V* curves shown in Figure 5.12 presents a semicircular pattern, which suggest their deviation from that of standard *P-V* characteristics, but the devices fill factor (*FF*) is noticed to increase from 26% to 27% and 29% once Alq3 and Gaq3 incorporated, respectively. It is claimed that *FF* can be limited by the unbalance of electrons and holes mobility in the active layer blends (D. Gupta, et al., 2010). Consequently, upon the incorporation of Mq3 into the DH6T:PCBM blend, the carrier transport is more balanced. This can prevent the hole accumulation and ultimately results in a larger *FF*.

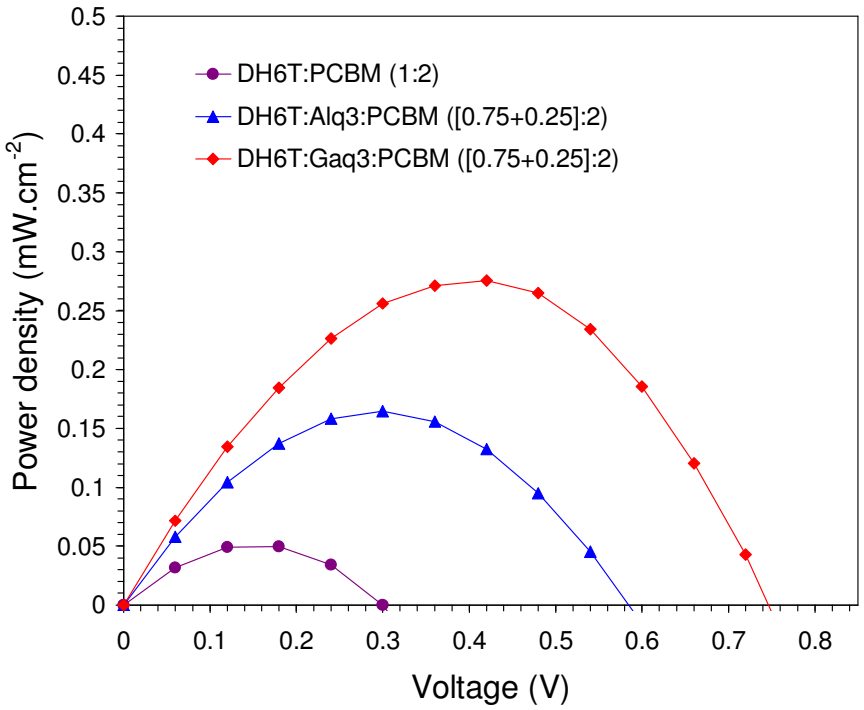

Figure 5.12: The *P–V* characteristics of the bulk heterojunction devices with and without incorporated Mq3.

5.4.2 Series and Parallel Resistances

As previously illustrated in Figure 2.3 of Chapter two, organic solar cell devices can be modeled by an equivalent circuit having two distinct resistances known as series (R_s) and shunt (or parallel) (R_{sh}) resistance. The values of R_s and R_{sh} can be extracted from the inverse gradient of the *J-V* results under light illumination in the specific regions. Figure 5.13 shows the photo *J-V* curve of the devices in the voltage range from -1 V to 2 V along with the regions where R_s and R_{sh} can be estimated. The values of R_s and R_{sh} are found from the inverse gradient of the *J-V* curve around the points where J_{sc} = 0 and V_{oc} = 0, respectively. From these calculations, as tabulated in Table 5.2, the value of R_s increased upon addition of Mq3 from 887 Ω to 985 Ω and from 887 Ω to 936 Ω for devices incorporating Alq3 and Gaq3, respectively compared to that of DH6T/PCBM device. The increment in R_s of the cells may be attributed to a small disruption in electron mobility upon the addition of Mq3, as Mq3 materials show lower

electron mobility compared to that of PCBM (Cai, et al., 2010; Koeppe & Sariciftci, 2006; Malliaras, Shen, & Dunlap, 2001). However, because of higher electron mobility of Gaq3 compared to that of Alq3 (Chena & Sun, 2003), the devices with Gaq3 is seen to attain lower R_s (936 Ω) compared to that of Alq3-based (985 Ω). Noteworthy, by incorporating Mq3, the value of R_{sh} is considerably increased from 5.5 kΩ to 6.2 kΩ and to 7.7 kΩ for Alq3 and Gaq3, respectively. This feature can be safely ascribed to the generation of new percolating pathways, helping the charge carriers to diffuse into longer distances before they geminately recombine, which is supported by the PL emission as discussed in Section 5.2.2. It is understandable that such R_{sh} increment will play a major role to reduce the leakage current, hence increasing I_{sc}, *FF* and the overall photovoltaic performance.

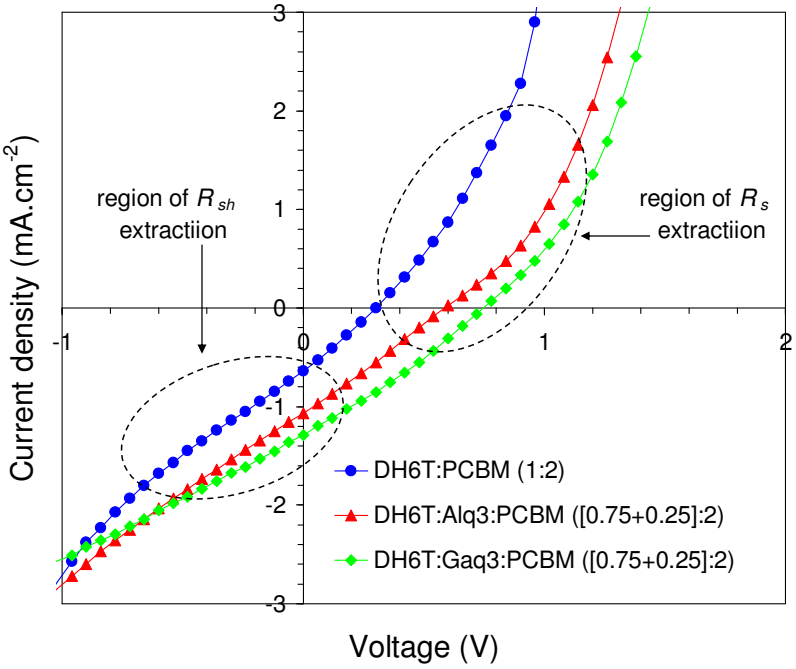

Figure 5.13: The *J–V* characteristics of the devices with and without incorporated Mq3, illustrating the regions where R_s and R_{sh} of the devices can be extracted.

Figure 5.14 shows the *J-V* characteristics of the devices in the dark and under light illumination in both of forward and reverse biased regions. It can be noticed that the shape of the curves in the far forward region is almost the same and no pronounced change can be observed when the devices are illuminated compared to those of the under dark devices. However, in contrast to this, the reverse biased part, the curves are observed to considerably shift downwards covering some parts of the near forward region, hence producing an interesting change in the *J-V* gradient. It is this significant shifting and *J-V* gradient that is recognized as to refer to the photovoltaic effect, thereby producing photocurrents upon illumination of light onto the devices. These behaviors even make the devices suitable to be applied as photodetectors.

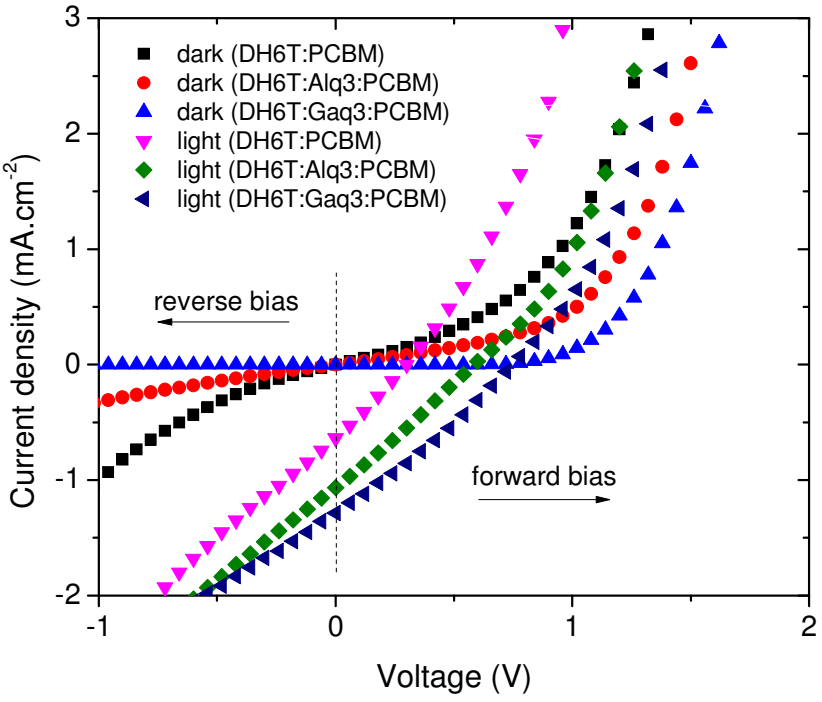

Figure 5.14: The influence of Mq3 in the D3HT:PCBM-based devices on *J–V* characteristics in the dark and upon light illumination.

Table 5.2: The photovoltaic and physical parameters of the solar cell devices obtained with and without incorporated Mq3.

Active layer structure	$J_{sc.}$ **(mA)**	$V_{oc.}$ **(V)**	R_s **(Ω)**	R_{sh} **(kΩ)**	***FF %***	***η %***
DH6T:PCBM (1:2)	0.63	0.30	887	5.5	26	0.06
DH6T:Alq3:PCBM ([0.75+0.25]:2)	1.06	0.60	985	6.2	27	0.21
DH6T:Gaq3:PCBM ([0.75+0.25]:2)	1.29	0.75	936	7.7	29	0.35

5.4.3 Equivalent Circuit and Charge Transport Properties

The parallel connection of a constant current source (I_{sc}) with an ideal diode that produces a voltage drop (V_{oc}) at open circuit condition can be modeled to an ideal organic solar cell (OSC) device. However, there is no such ideality feature in the real photovoltaic characteristics of OSCs. Hence, a series (R_s) and parallel (R_{sh}) resistance should be connected additionally to approach a real solar cell behavior. The equivalent circuit of these devices is illustrated in Figure 2.3, while their electrical characteristics can be analyzed and understood by considering their *J-V* curves. Figure 5.15 shows the semilog plot of *J-V* curve for a representative device under the dark and illuminated conditions. It can be seen that by applying a potential difference across the device in the dark (absence of light), the device behaves like a normal diode, where at the zero biased voltage no pronounced current is passing through the device. However, by increasing the voltage to beyond a specific voltage ($\approx V_{oc}$) forwardly (positive and negative voltages applied to the ITO and Al electrodes, respectively), the current is considerably increased. It is this voltage that the incident photons have to attain in order that they are able to overcome (off set) the diode potential barrier (V_{oc}), and hence generating a significant photocurrent (I_{sc}) during illumination. These situations can be clearly seen in Figure 5.15, where by applying a voltage close to V_{oc}, the photocurrent is minimized to the lowest point, while compared to the zero biased volts, a maximum photocurrent (I_{sc}) is generated within the device that is capable to pass through the output load. One can notice that under illumination, the current to voltage ratio (rectification ratio) at high

voltages is decreased compared to that of the dark condition. It has been suggested that this is due to the photoconductivity, where the number of charge carriers participating in the conduction of current increases from the dissociation of excitons at expended D/A interfaces (Sharma, et al., 2008), thereby acting as reverse passage current compared to that generated due to the external applied voltage.

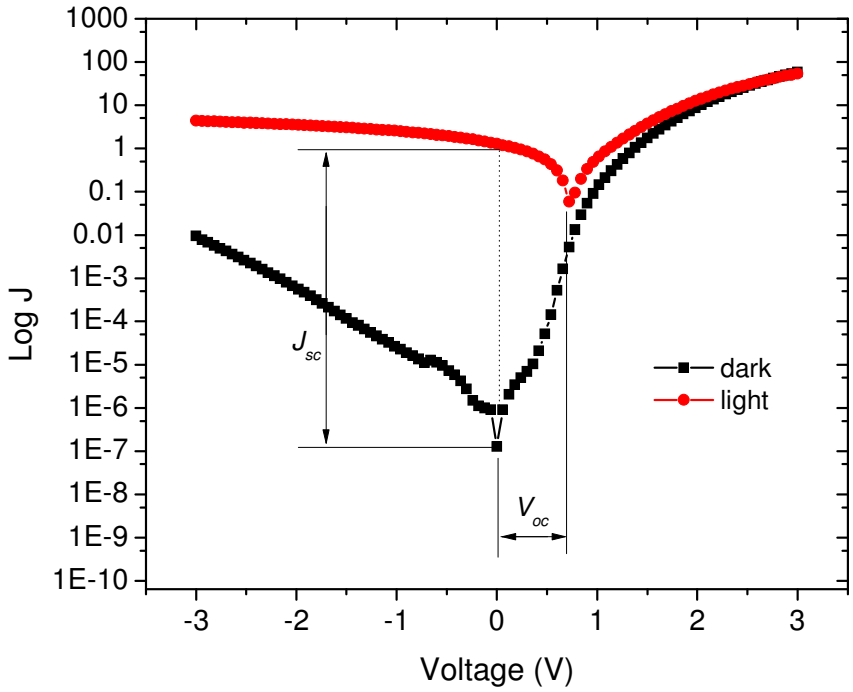

Figure 5.15: The light and dark semi log *J–V* characteristics of a representative device under investigation.

Figure 5.16 shows the double log *J–V* characteristics of the devices with and without incorporated Mq3 in dark condition. It can be noticed that for all devices, at low voltages the current is varied approximately linearly with the applied voltage ($J \propto V^{1.2}$) as observed in region A (ohmic regime). In region B, the current becomes space charge limited (SCLC) due to the presence of traps, and therefore is proportional to the square of the applied voltage ($J \propto V^2$) (Schön, et al., 2001). The region where the slope of the curve is higher than two can be described as a trap-filling space charge limited current (TFSCLC) region and charge are injected into the bulk of active layer (Sharma, et al.,

2008; Sulaiman & Fakir, 2011). In this region charge injection into the device occurs by tunneling and the bulk is able to use up all the injected charges in the conduction of current, until such a point where the bulk becomes saturated, and injected charges start to accumulate near the injected electrode. In region C, the rate of increasing current with voltage decreases (as the current approaches to $J \propto V^5$). This is due to the fact that all possible traps are filled and current approaches the trap-free SCLC. It should be pointed out that the SCLC region is hardly observed in the DH6T/Gaq3/PCBM-based for the reason that the traps become filled rapidly and the current rises by many orders of magnitude ($J \propto V^{10.8}$) in this Mq3 incorporated device. While the DH6T/PCBM based devices exhibited the expected dependence of current density on V^2, these results suggest that Mq3 incorporated devices possess the improved exciton dissociation and lower trap densities.

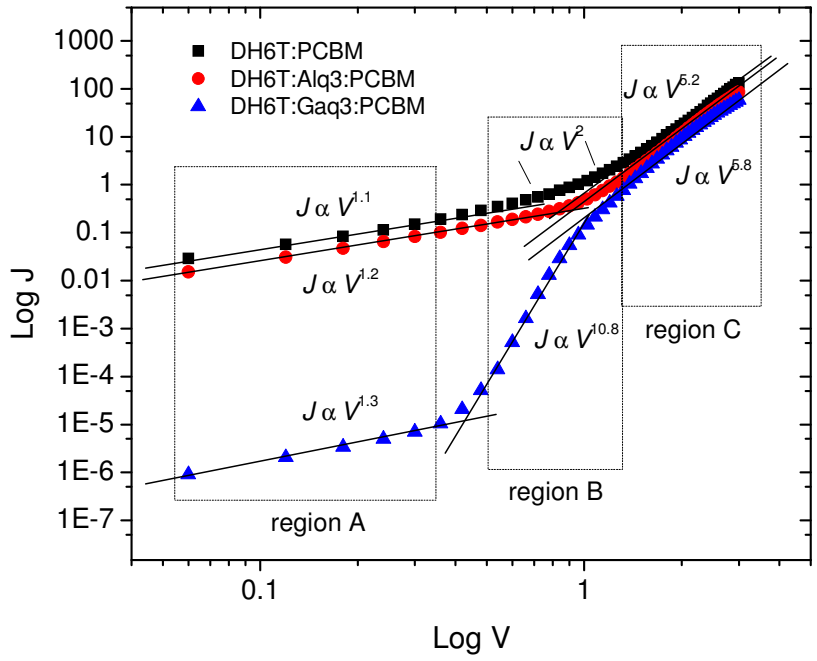

Figure 5.16: The double logarithmic plot of *J–V* characteristics for the devices with and without incorporated Mq3 in the dark condition.

Figure 5.17 shows the semi-log *J–V* characteristic of a representative device in the dark condition, while its inset depicts the equivalent circuit of OSCs. In this figure, three regions can be easily identified: Region 1 with a linear region at low forward bias voltages, where the current is limited by the shunt resistance (R_{sh}). This region continues to occur exist up to the point where the applied voltage approaching the potential barrier (V_f) of the diode; Region 2 with an exponential behavior at intermediate forward bias voltages where the current is controlled by the diode, and finally region 3 with a second linear dependence at high voltages where the current is limited by the series resistance (R_s). A higher R_{sh} value causes a lower leakage current, whereas a higher R_s value produces lower rectification behavior; thereby the larger photocurrent is gained in the device. Due to these, in the organic solar cells, the achievement on higher R_{sh} and lower R_s values are usually targeted.

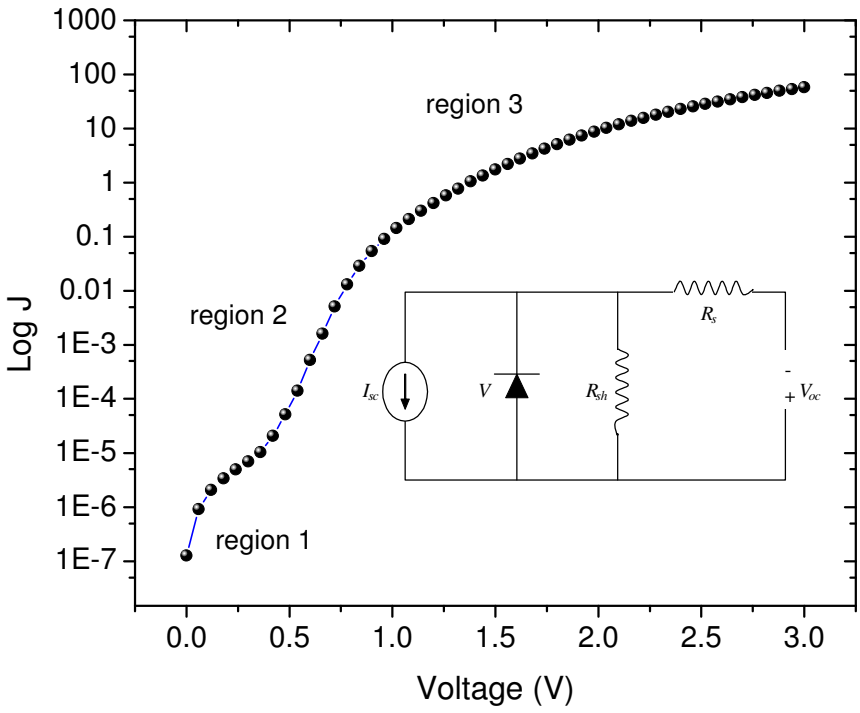

Figure 5.17: The semi-log *J–V* characteristic of a representative device in the dark condition; inset of the Figure depicts the equivalent circuit of OSCs.

5.5 Summary

In summary, DH6T films have been doped with various weight percentages of Mq3 to investigate its impact on the DH6T:Mq3 blends absorption edge energies (E_g). From the results analysis and by applying an empirical formula to fit the variation of the absorption band gap, 25% of Mq3 is found to be the optimum amount for the organic solar cells application. The photoabsorption spectra of DH6T/Mq3/PCBM ternary bulk heterojunction blends upon incorporating the optimum amount of Mq3 reveal a considerable broadening in the absorption spectra of the films. In addition, the PL quenching behaviors of the same ternary blend support the absorption results, which provide evidence as Mq3 strong candidate for solution-processed organic solar cells. Having obtained information on the photophysical of the blend films, devices based on bilayer (BL) and bulk heterojunction (BHJ) active layers of DH6T/PCBM have been assessed. The results of the BHJ structure demonstrated an improved photovoltaic performance by a factor of 1.5 better than that of the BL structure. Nevertheless, it is found that the fill factor (*FF*) in the BHJ devices is lower compared to that of BL ones. Such phenomenon is ascribed to the deviation in the *P-V* curves, which is thought to be originated from the morphology complexity of the D/A phases. Consequently, the D/A blend structures are selected as the favored system to incorporate the optimum amount of Mq3 materials. Finally, the influence of Mq3 in the DH6T/Mq3/PCBM based devices on the electrical characterizations has been investigated. The *J-V* and *P-V* characteristics analysis in dark and under illumination demonstrate that the photocurrent, open circuit voltage, and the entire performance of the devices by a factor of approximately six (6) times greater in the Mq3 incorporated device than those without Mq3. Moreover, the devices equivalent circuit and their charge transport properties have been analyzed and discussed.